

Polaron formation in Bi-deficient BaBiO₃

W. Román Acevedo,^{1,2} S. Di Napoli^{1,2}, F. Romano,^{1,2,3} G. Rodríguez Ruiz^{1,2,3}, P. Nukala^{4,5}, C. Quinteros,⁵ J. Lecourt,⁶ U. Lüders,⁶ V. Vildosola^{1,2} and D. Rubi^{1,2}

¹Departamento de Física de la Materia Condensada, GIYA-CNEA, Av. General Paz 1499, (1650) San Martín, Pcia. de Buenos Aires, Argentina

²Instituto de Nanociencia y Nanotecnología (INN CNEA-CONICET), 1650 San Martín, Argentina

³Depto. de Física, FCEyN, Universidad de Buenos Aires, Pab I, Ciudad Universitaria, Buenos Aires (1428), Argentina

⁴Center for Nanoscience and Engineering, Indian Institute of Science, Bangalore 560012, India

⁵Zernike Institute for Advanced Materials, University of Groningen, 9747AG The Netherlands

⁶CRISMAT, CNRS UMR 6508, ENSICAEN, 6 Boulevard Maréchal Juin, F-14050 Caen Cedex 4, France



(Received 10 April 2021; revised 8 July 2021; accepted 13 September 2021; published 23 September 2021)

BaBiO₃ is a charged ordered Peierls-like perovskite well known for its superconducting properties upon K or Pb doping. We present a study on the transport and electronic properties of BaBiO₃ perovskite with strong Bi deficiency. We show that it is possible to synthesize BaBiO₃ thin layers with Bi vacancies above 8–10% by depositing an yttrium-stabilized zirconia capping layer. By combining transport measurements with *ab initio* calculations we propose a scenario where the Bi vacancies give rise to the formation of polarons and suggest that the electrical transport is dominated by the migration of these polarons trapped at Bi³⁺ sites. Our paper shows that cation vacancies engineering, hardly explored to date, appears as a promising pathway to tune the electronic and functional properties of perovskites.

DOI: [10.1103/PhysRevB.104.125307](https://doi.org/10.1103/PhysRevB.104.125307)

I. INTRODUCTION

Perovskite oxides display a plethora of physical properties, such as magnetism [1], ferroelectricity [2], and/or superconductivity [3], making them attractive materials for the development of sensing [4], information storage [5], or computing devices [6], among others. The possibility of implementing these devices has boosted in the last decades as oxide thin films and heterostructures with excellent crystalline properties, chemistry, and atomically controlled surfaces and interfaces have been developed. Defects are ubiquitously found in oxide thin films, oxygen vacancies being the most common ones [7]. Cationic vacancies have been less studied due to their lower concentration in comparison with oxygen vacancies [8], but they might have a significant impact on the physical properties of the films as they could strongly modify the oxide electronic structure.

BaBiO₃ (BBO) is a perovskite, which becomes superconducting upon Pb or K doping [9,10] with high critical temperatures up to ~30 K. Pristine BBO is an insulator due to the existence of a charge ordered state comprising Bi ions with formal +3 and +5 valences [11]. This is accompanied with structural distortions involving both the so-called breathing distortions and tiltings of BiO₆ octahedra [12], which reduces the high-temperature cubic crystal symmetry to a monoclinic structure at room temperature. Bi-O bond distances have been reported as 2.11 and 2.29 Å, respectively [12]. Spectroscopic experiments have failed to resolve valence differences between Bi ions in both crystallographic sites [13,14], while theoretical work suggests a common ≈ +3 state, which has been rationalized in terms of spatially extended Bi-O bonds related to hybridized Bi-6*s* and O-2*p* atomic orbitals [15–17]. BBO has been proposed to behave as a topological insulator

upon electron doping [18], and it was also theoretically suggested to present a 2D electron gas in its Bi-terminated (001) surface [19]. Moreover, 2D superconductivity has been shown at the BBO/BaPbO₃ interface [20,21].

Reports on BBO thin films are scarce [22–31]. Most papers report on the growth and properties of BBO on SrTiO₃ (STO) substrates [22,23,25,28–31], with both materials presenting a rather large lattice mismatch of ≈ 12%. It was shown that this misfit is accommodated through the formation of an ultrathin interfacial δ-Bi₂O₃ layer with a fluorite structure, which forms a coherent interface with the substrate and a semi-coherent interface with BBO [28,31]. Recent reports indicate that the electronic structure of BBO on STO is thickness dependent and is affected by chemical and structural effects imposed by the substrate/film interface [29,32]. These results indicate that substrate effects on the BBO electronic structure might not be disregarded in thin epitaxial films.

With the aim of studying the effect of (B-site) Bi deficiency on the electronic and transport properties of BBO, we have developed a fabrication procedure allowing for the introduction of a large amount of Bi vacancies in stoichiometric BBO thin films on silicon. From a combination of experiments and *ab initio* calculations, it is proposed that Bi deficiency leads to the formation of polarons that dominate the electrical transport. Our paper shows the control of cation deficiency as an emerging degree of freedom that allows tuning the BBO electronic structure and its functional properties.

II. EXPERIMENTAL SECTION

BBO thin films were deposited by pulsed laser deposition using a Nd-YAG Spectra Physics laser with $\lambda = 266$ nm

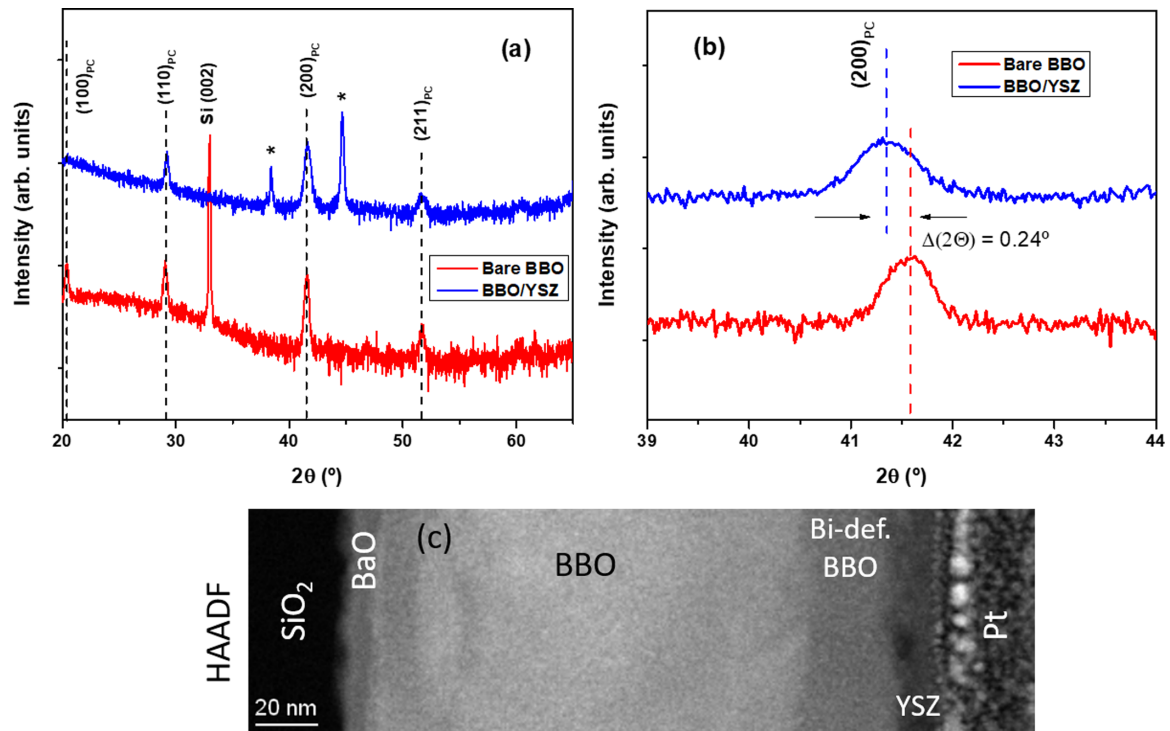


FIG. 1. (a) X-ray diffraction spectra corresponding to both bare and capped BBO. Peaks indexes correspond to the pseudo-cubic (PC) perovskite BBO lattice. Peaks marked with * correspond to the sample holder used for the measurement of the capped BBO sample [35]. Zero-shift corrections were made from the position of Si peaks. (b) Blow-up of the spectra displayed in (a), evidencing the shift of diffraction peaks to lower angles for capped BBO. Maxima are shifted by 0.24° . Also, capped BBO displayed broader diffraction peaks (FWHM of $\approx 0.5^\circ$ and $\approx 0.7^\circ$ for BBO and capped BBO, respectively) with a slight asymmetry. (c) TEM HAADF image corresponding to a BBO/YSZ bilayer on Si/SiO₂, with the YSZ grown at an oxygen pressure of 0.1 mbar. The Pt layer on top of the YSZ layer was deposited for the lamella preparation.

and 850 mJ per pulse. Structural characterization of the films was performed by means of x-ray diffraction (XRD) using two Panalytical Empyrean diffractometers with PIXcel ultrafast detectors, in standard Bragg-Brentano configuration (0.02° steps were used for 2θ scanning). Transmission electron microscopy (TEM) was performed with a Thermo Fisher Scientific Themis Z monochromated and double corrected microscope operated at 300 kV.

In order to get Bi-deficient BBO, we followed this procedure: First, we deposited a stoichiometric BBO film (≈ 165 nm thick) on commercial Si/SiO₂ substrate, at a temperature and oxygen pressure of 550°C and 0.01 mbar, respectively. We chose this substrate in order to obtain strain-free polycrystalline films, as will be shown below. Next, we deposited (*in situ*), on top of BBO, a yttrium stabilized zirconia (YSZ, ≈ 17 nm thick) capping layer, at room temperature, at an optimized oxygen pressure of 0.1 mbar. YSZ is a well-known oxygen conductor [33] but has also been reported to display high cationic conductivities [34]. In our case, under the proper deposition conditions, YSZ capping favours the diffusion of Bi from BBO to YSZ, leading to an interfacial BBO layer with a strong Bi deficiency.

Figure 1(a) shows x-ray diffraction spectra recorded for both bare and capped BBO films. It is found in both cases the presence of peaks corresponding to the BBO perovskite structure while, for capped BBO, YSZ remains amorphous. BBO peaks were indexed considering a pseudo-cubic (PC)

lattice. We extracted a cell parameter for bare BBO $a_{PC} = 4.339(5)$ Å, in excellent agreement with the value corresponding to bulk BBO (4.335 Å). Upon YSZ capping, there is a shift of x-ray peaks towards lower angles [see Fig. 1(b)], reflecting an (average) BBO unit-cell parameter expansion of $\approx 0.5\%$. This is a first indication of the formation of Bi vacancies at the BBO layer, as unit-cell enlargement is a signature of B-site vacancies in perovskites [36–38]. We will come back later to this issue.

Figure 1(e) displays a HAADF-STEM cross section of a capped BBO film. First we notice the existence of a thin BaO layer (≈ 11 nm, undetectable by XRD) at the substrate/BBO interface, confirmed by the EDS maps shown within the Supplemental Material [35]. This interfacial BaO layer has been observed before in BBO thin films [27] and can be related to the poor sticking coefficient of Bi ions during the first growth stages [29,39]. Next, Fig. 1(c) displays a BBO layer divided in two zones with different contrast, the darker one (≈ 30 nm thick) located at the interface with YSZ. As HAADF brightness is higher for species with high atomic number such as Bi, the darker BBO fringe is an indication of Bi-deficiency at this zone. We notice that it is difficult to perform a precise composition quantification, as during EDS mapping we observed some grain growth together with changes in the HAADF contrast between BBO and Bi deficient BBO [35], indicating Bi diffusion during the measurement. With this constraint in mind, we can roughly estimate a lower bound

of $\approx 8\text{--}10\%$ of Bi vacancies at the Bi-deficient BBO layer [35]. This statement is supported from the analysis of $(200)_{PC}$ x-ray peaks shown in the Supplemental Material [35]. The $(200)_{PC}$ reflection of bare BBO can be fitted with a single Gaussian component, centered at $2\theta = 41.59^\circ$, corresponding to a bulk-like cell parameter $4.339(5)$ Å. On the other hand, the capped BBO $(200)_{PC}$ reflection shows a broadened peak with a slight asymmetry. The peak can be deconvoluted by assuming two Gaussian contributions centered at $2\theta = 41.59^\circ$ and $2\theta = 41.25^\circ$. These two components are attributed to BBO and Bi-deficient BBO, with cell parameters $4.339(5)$ Å and $4.374(5)$ Å, respectively. The latter cell parameter accounts for a ≈ 4 pm BBO cell expansion due to the presence of Bi vacancies. We recall that in the case of Ti-deficient SrTiO₃ such expansion corresponds to a 10–15% B-cation deficiency [36], allowing an additional estimation of the amount of B-site vacancies in the Bi-deficient layer of capped BBO, which is consistent with the previous one obtained from microscopy analysis. We also notice that the formation of Bi vacancies might be concomitant with the formation of oxygen vacancies. However, this hypothesis can be discarded as the cross-section TEM-EDS oxygen map recorded on the YSZ-capped BBO sample [35] does not show a diminished signal intensity for the Bi-deficient BBO layer in relation to the BBO one.

Now we will focus on the electrical transport properties of our samples. BBO single crystals were reported to display an insulating, thermally activated behavior [40]. Transport properties in BBO thin films have been rarely published: some authors reported an “insulating behavior” [24] in BBO thin films on MgO but no temperature-dependent resistivity was shown, while a negative resistance coefficient, in the range 200–300 K, was displayed for BBO films on silicon [26]. We recall that the transport properties in semiconducting oxide thin films can be highly affected by the presence of defects. For instance, BaSnO₃ thin films were shown to present dramatic changes in their resistivity values and the corresponding temperature behavior depending on the films’ free carriers concentration [41], strongly linked to the type and number of existing defects.

Electrical transport has been measured on the deposited structures at low temperatures (50–200 K) in a 4-point configuration using a multipurpose Quantum Design Versalab cryostat. In order to gain electrical access to the capped BBO samples, we have covered some parts of the substrate by shadows masks during the deposition [Fig. 2(b)]. Electrical contacts were fixed with silver paste. Figure 2(c) displays the evolution of the 4-points resistance versus temperature for both uncapped and capped BBO films. Bare BBO films show a resistance nearly independent of the temperature in the measured temperature range indicating that the expected thermally activated behavior (negative resistance coefficient) is compensated with a reduction of carriers mobility as temperature increases. We note that the mentioned behavior of the mobility with temperature implies that mobility is limited by phonons rather than by impurity scattering, this balance being very sensitive to free carriers density [42]. On the other hand, capped BBO shows lower resistance values—a 6-fold decrease at 175 K—together with a semiconducting-like behavior characterized by a decrease of the resistance as the temperature increases. We checked in separate control experiments that

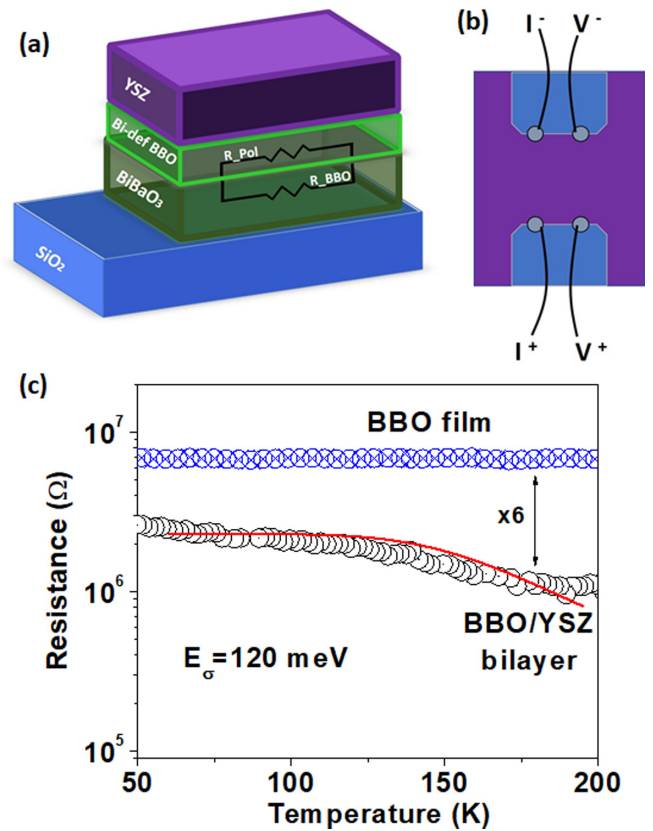


FIG. 2. Sketches showing (a) the SiO₂/BBO/Bi-def. BBO/YSZ stack and (b) a top view of the contacted device. Small parts of SiO₂ (top layer of the substrate, blue) were left exposed in order to access the BBO and Bi-deficient BBO layers for 4-points transport measurements. Same colors are used for (a) and (b). (c) 4-points resistance as a function of the temperature recorded for a bare BBO film and a YSZ-capped heterostructure. The red line shows a fitting assuming a polaronic conduction model for the Bi-deficient BBO layer (see text for details).

both SiO₂ and YSZ present resistances several orders of magnitude higher than those shown in Fig. 2(c) and this is also the case for the estimated resistance corresponding to the BaO layer (>10 GΩ), given its reported resistivity ($\approx 10^4$ Ωcm at ≈ 700 °C) and semiconducting-like temperature behavior [43]. Therefore we can safely exclude the contribution of these three layers to the electrical transport and assume that, for capped BBO, the electrical transport flows through two parallel channels related to BBO and Bi-deficient BBO layers [see the sketch of Fig. 2(a)]. This scenario was considered to fit the experimental data by proposing an equivalent circuit formed by a temperature-independent resistance R_{BBO} for the BBO layer in parallel with a polaronic transport channel, attributed to the Bi-deficient BBO layer, with a temperature-dependent resistance $R_{Pol}(T)$ given by [44]

$$R_{Pol}(T) = \frac{K_0 a}{g_d e^2 v_0} k_B T \exp\left(\frac{E_\sigma}{k_B T}\right), \quad (1)$$

where k_B is the Boltzmann constant, T is the absolute temperature, e is the electronic charge, a is the polaron hopping distance, v_0 is the jump attempt frequency related to the phonon vibrations coupled to the polaron, E_σ is the activation

energy for polaron hopping, g_d is an adimensional factor that depends on the hopping geometry [45] and $K_0 = L/Wt$, with L , W , and t being the length, width, and thickness of the Bi-deficient BBO layer, respectively.

The $R(T)$ for the bilayer is thus given by

$$R(T) = \frac{R_{BBO}R_{Pol}(T)}{R_{BBO} + R_{Pol}(T)}. \quad (2)$$

The fitting of $R(T)$ is shown with a red full line in Fig. 2(c) and displays a reasonable agreement with the experimental data for $E_\sigma = 0.12$ eV and $K_0 \frac{ak_B}{g_d e^2 v_0} = 5.0 \Omega/K$.

If we take $v_0 = 1.710^{13}$ Hz (the breathing mode vibration frequency [46]), $a = 0.437$ nm corresponding to this perovskite cell parameter, $g_d = 3/8$ [47] and $K_0 = 0.067 \text{ nm}^{-1}$ ($L/W \approx 2$ given by our sample geometry and $t = 30$ nm, as extracted from the TEM analysis of Fig. 1) we obtain a theoretical value $K_0 \frac{ak_B}{g_d e^2 v_0} = 2.5 \Omega/K$, in very good agreement with the fitted value, giving consistency to our analysis.

We recall that it has been theoretically proposed that, upon hole doping, BBO remains insulating due to the coupling between holes and phonons [48] and the subsequent formation of polarons. This is likely the case of Bi-deficient BBO, where the holes for polaron formation are provided by Bi vacancies, as it will be analyzed in the next section by means of first principles calculations.

III. DFT CALCULATIONS

To study the different physical mechanisms that could trigger the transport properties of Bi-deficient BaBiO_3 , we perform *ab initio* calculations within the framework of density functional theory (DFT) and the projector augmented wave (PAW) method [49], as implemented in the Vienna *ab initio* package (VASP 5.4.1) [50,51]. We explicitly treat 10 valence electrons for Ba ($5s^2 5p^6 6s^2$), 15 for Bi ($5d^{10} 6s^2 6p^3$), and 6 for O ($2s^2 2p^4$) [52]. To properly describe the electronic structure of charge ordered and semiconducting BaBiO_3 specially in the presence of localized defects, it is necessary to consider long-range exchange interactions that are poorly described by the standard local and semilocal functionals as the local density approximation (LDA) or the general gradient approximation (GGA). Therefore, we use the semilocal functionals developed by Perdew, Burke, and Ernzerhof (PBE) [53] and we add the hybrid functional including a fraction of nonlocal Hartree-Fock exchange interactions through the Heyd-Scuseria-Ernzerhof (HSE06) functionals [54,55] in all the calculations to avoid spurious metallic states.

The charge-ordered phase of BaBiO_3 is represented formally by the $\text{Ba}_2^{+2}\text{Bi}^{+3}\text{Bi}^{+5}\text{O}_6^{-2}$ formula unit. The two Bi species are ordered in an alternated way within a monoclinic $I2/m$ structure [11]. In the present paper, we describe the Bi-deficient system by removing neutral Bi atoms from BBO bulk supercells of different sizes and perform spin-polarized calculations to allow for unpaired bonds. To compute the electronic properties of perfect BaBiO_3 and Bi-deficient $\text{BaBi}_{0.75}\text{O}_3$, containing a 25% of Bi vacancies, we use a supercell rotated 45° with respect to the simple cubic single perovskite and which contains 4 Bi sites in total, 2 per layer and two planes in the z direction. To explore lower

concentrations of Bi vacancies we also perform calculations in a $2 \times 2 \times 2$ FCC supercell containing 80 atoms [56], as the one used in Ref. [48]. This larger supercell contains 16 Bi atoms per unit cell and allows us to account for defect concentrations of 12.5% (2 Bi vacancies) and 18.75% (3 Bi vacancies).

The HSE calculations within the smaller unit cell are performed using a 450 eV energy cutoff in the plane waves basis and to evaluate the integrals within the Brillouin zone (BZ), a $4 \times 4 \times 3$ Monkhorst-Pack k -point grid is employed. The corresponding values for the energy cutoff and k -points grid in the larger FCC supercell are 400 eV and $2 \times 2 \times 2$, respectively. The experimental lattice parameters [11] are used in all the calculations and internal structural relaxations are performed until the forces on each ion are less than 0.02 eV/\AA [57].

For perfect BaBiO_3 , our calculations predict the semiconducting state with a band gap of 0.90 eV, exhibiting the charge disproportionation between the two different species, Bi^{+3} and Bi^{+5} in agreement with previous calculations [58]. In Fig. 3(a) we show the corresponding band structure where the full $6s$ bands of Bi^{+3} are depicted in red and the empty ones of Bi^{+5} are in dark green. It is important to mention that the Bi-O bonds can be described by spatially extended hybridized $6s$ - $2p$ orbitals and all the bands present a strong s - p hybridization. The color coding used in Fig. 3 and in the following ones is just a guide to the eye.

Distinct kinds of defects appear in the presence of Bi vacancies. It is worth to mention that several molecular dynamics steps, followed by relaxation, were necessary to stabilize these defects in order to avoid spurious metallic solutions [48]. In the following, we describe the results obtained for the different Bi vacancies concentrations considered.

The system with 25% of Bi-vacancy concentration has been simulated in the small cell where one out of four Bi is withdrawn. Independent of the site of the vacancy, whether it is at a Bi^{+5} or Bi^{+3} site, the resulting electronic structure is very similar. For instance, if the vacancy is at a Bi^{+5} site, in order to compensate the lacking five electrons, each of the remaining two Bi^{+3} liberates two electrons, so that the originally full $6s$ bands become empty. These two trapped holes at each Bi^{+3} form a bipolaron. Since the remaining Bi^{+5} site has its $6s$ band already empty, the other missing electron turns into a hole trapped at the surrounding oxygen cloud next to the Bi vacancy. On the other way around, if the vacancy is at a Bi^{+3} site, the lacking three electrons give rise to a bipolaron at the remaining Bi^{+3} site and a hole trapped at the oxygen p -bands surrounding the vacancy. In Fig. 3(b) we show the electronic band structure, with the orange narrow band corresponding to holes trapped at the oxygen cloud around the vacancy, whose charge density is depicted in Fig. 4(a). The bands in blue are the bipolarons with the corresponding charge density shown in Fig. 4(b).

As mentioned before, the systems with 12.5% and 18.5% Bi vacancy concentrations have been simulated with a supercell containing 16 Bi sites. In the case with an even amount of vacancies, the kind of electronic defects are only of the bipolaron type.

In Fig. 3(c), we show the calculated electronic band structure obtained for the 12.5% concentration, where there are two vacancies at Bi^{+3} sites in the unit cell. The three occupied bands in red are the full $6s$ bands of the remaining Bi^{+3} , the

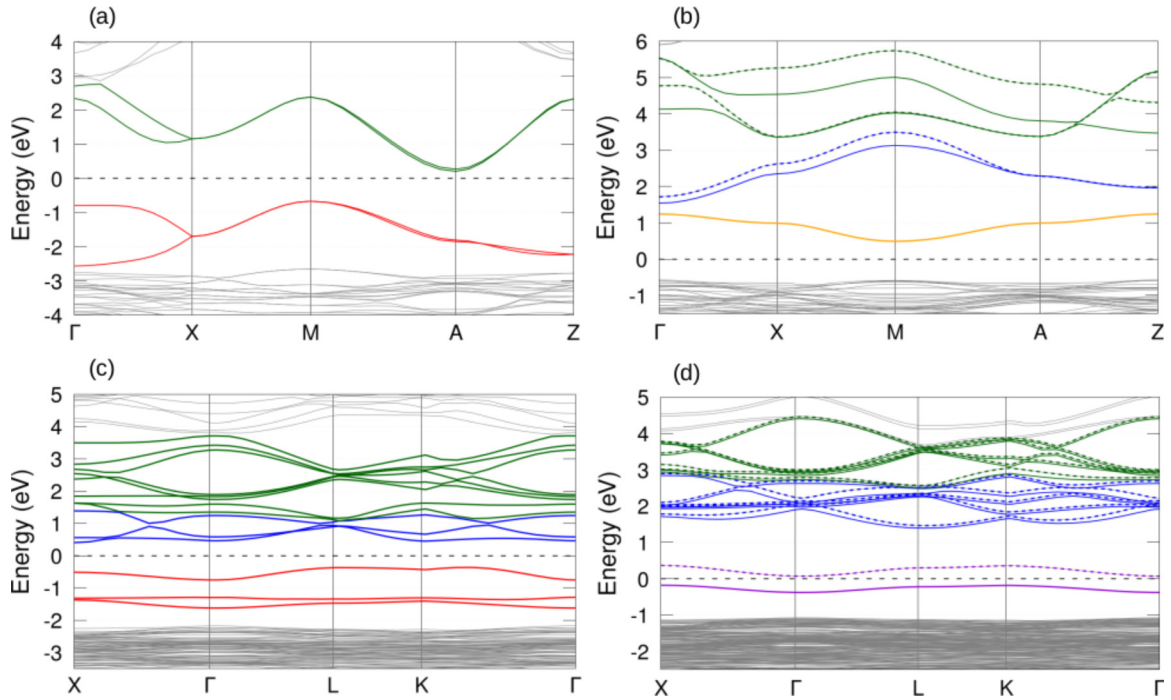


FIG. 3. Spin-polarized band structure of (a) perfect BaBiO₃ and Bi-deficient BaBiO₃ with (b) 25%, (c) 12.5%, and (d) 18.75% of Bi-vacancies. Solid lines correspond to spin-up projection and dashed lines to spin-down. In (a) and (c) spin-up and spin-down bands are degenerate. Red bands correspond to Bi⁺³, dark-green ones to original Bi⁺⁵ atoms, and blue to created bipolarons. The orange band in (b) represents the hole trapped at the oxygen cloud centered at the Bi-vacancy sketched in Fig. 4 (a) and the violet bands in (d) correspond to the charge/hole polaron originated around Bi₁₂ [see text and Fig. 6(b)].

three bands in blue are those of the bipolarons, and, at higher energies, the eight *s* bands of the Bi⁺⁵ are in dark-green. In the case of even number of vacancies, the system is non-spin polarized so that the bands are doubly degenerate.

When the Bi vacancy concentration is 18.75%, there are three vacancies in the supercell. For example, if two of the vacancies are at a Bi⁺³ site and the other one at a Bi⁺⁵, there are eleven electrons missing. The six remaining Bi⁺³ sites can provide this charge. That is, five of these Bi⁺³ sites turn into Bi⁺⁵ by trapping two holes each giving rise to five bipolarons [blue bands in Fig. 3(d)]. The remaining Bi⁺³ keeps one elec-

tron forming a polaron with a localized spin-polarized charge [violet band in Fig. 3(d)].

In order to analyze the role played by each type of defects into the transport properties we proceed to estimate the activated diffusion barrier E_σ in each case.

The hole polaron trapped at the *p* bands of the oxygens that surround the Bi vacancy in the highly doped case (25% vacancy concentration), is a mixed type of defect where the Bi vacancy is bound to a hole electronic cloud. The nudged elastic bands (NEB) [59] method has been used to estimate the activation barrier, taking into account two different migration pathways (see Fig. 5). The first one considers the migration of the defect within the *ab* plane, that is in the plane that contains the part of the hole shared by the 4 in-plane oxygen atoms. The second considered path was with the defect traveling along the (111)-(111) direction, with the inflection point located at an optimized height. That is, the defect traveling from the (1/2, 1/2, 1/2) to the (0,0,0) position, through (1/4,1/4,*h*₀), being *h*₀ the optimized distance in the *z* direction from the *ab* plane. As shown in Fig. 5, we obtain $E_\sigma = 9.35$ eV and 4.9 eV, respectively. In view of these results, we conclude that the contribution to the electronic conductivity of these type of mixed defects is negligible.

To estimate the maximum of the energy barrier of the polaron and bipolaron trapped at Bi⁺³ sites (violet and blue bands of Fig. 3, respectively), we perform a static calculation for a transition state, where the lattice distortion coupled to the defect is transferred to an intermediate situation that forces the trapped charge to be equally distributed between neighboring Bi sites.

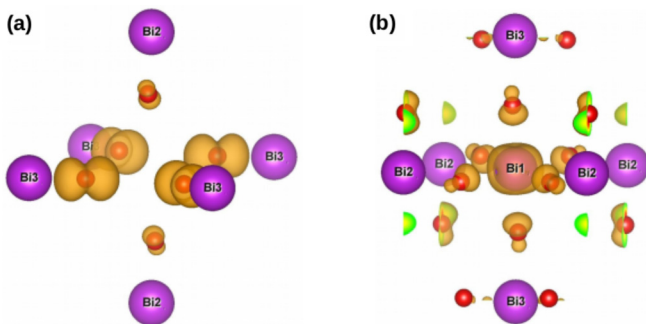


FIG. 4. Charge density plots of Bi-deficient BaBiO₃ with a 25% of Bi vacancies. Panel (a) shows the hole trapped at the oxygen cloud around the vacancy, corresponding to the orange band depicted in Fig. 3(b). The charge density shown in (b) corresponds to the bipolaron at the remaining Bi⁺³ site [blue band in Fig. 3(b)].

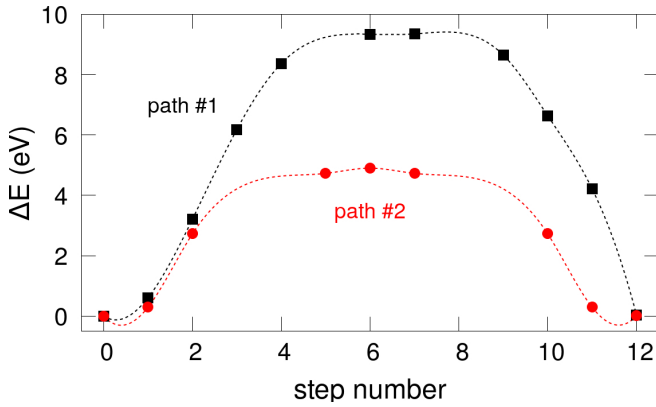


FIG. 5. Activation barrier of the hole polaron trapped at the oxygen p -bands that surround the Bi vacancy in the highly doped case, i.e., the 25% concentration of Bi vacancies. The barrier is calculated using NEB taking into account two different migration pathways (see text for details).

For the case with 18.75% Bi vacancy concentration, in the top panel of Fig. 6(a), we show the partial density of states (PDOS) projected onto the s -orbitals of two Bi neighboring sites, one of them trapping the polaron (labeled as Bi₁₂) and the other one belongs to a Bi⁺⁵, named Bi₅. The corresponding charge density associated with the polaron is shown in Fig. 6(b). In the bottom panel of Fig. 6(a), we plot the PDOS projected on the same Bi sites but in the situation where the polaronic charge is shared in equal parts between them. In Fig. 6(c) we show the related charge density. The energy difference between the initial and the intermediate situation provides an estimation of E_σ , that is 0.54 eV. When this approach is done to estimate E_σ for the bipolaron migration, where now two holes are hopping simultaneously, we obtain $E_\sigma = 0.60$ eV.

Interestingly, it is not surprising that this energy scale is related to the electron-phonon coupling in BBO systems, specially with the breathing phonon modes that are strongly correlated to Bi⁺⁵-Bi⁺³ charge ordering. The value around 0.5 eV for E_σ is of the same order of magnitude as the energy shift induced in the electronic bands when frozen phonon perturbations for the breathing mode are performed for bulk BBO [60]. However, as it has been recently reported in Ref. [21], this value decreases to ~ 0.2 eV in confined situations as the one described for the BBO/BaPbO₃ interface. So, it is likely that the value of ~ 0.5 eV obtained for the bulk supercell described here is overestimated since it does not take into account the confinement effects present in the real samples. Therefore, we consider that the actual activation energy might be close to the 0.12 eV obtained from the transport experiments and that the migration of polarons trapped at Bi⁺³ sites plays an important role in the increment of the electrical conductivity with the temperature, experimentally observed in our Bi deficient films.

It is worth mentioning that in this paper we study the effect of neutral Bi vacancies. The formation of charged defects during the synthesis of perovskites is usually accompanied by the creation of counter-charged defects in order to warrant overall charge neutrality. In our case, the formation of charged Bi vacancies should be accompanied with charged oxygen

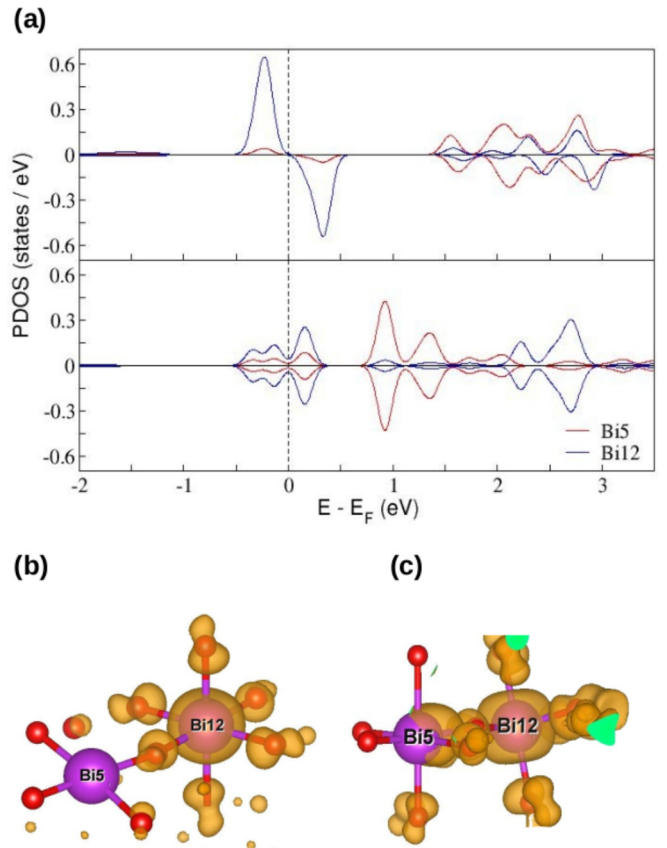


FIG. 6. [(a) Top panel] PDOS projected onto the s orbitals of two selected Bi atoms, the one with the polaron, i.e., Bi₁₂ and one of its nearest Bi neighbors, i.e., Bi₅. [(a) Bottom panel] PDOS projected onto the same Bi atoms for the intermediate situation where the polaronic charge is half-transferred between neighboring sites. (b) Charge-density plot corresponding to the localized state close to E_F shown in the top panel of (a), i.e., the polaron centered at Bi₁₂. (c) Idem (b) after the static perturbation where the polaronic charge is shared with Bi₅.

ones. However, as mentioned above, in our BBO films there are no signs of the presence of a large amount of oxygen vacancies. The main chemical difference between the bare and the YSZ-capped BBO films is the amount of Bi atoms so that the Bi vacancies are expected to be neutral. Still, in a system under electrical bias these defects could become charged. Nevertheless, we do not expect other electronic defects than hole polarons and bipolarons out of charged Bi vacancies. Moreover, their activation barrier would be dominated by the electron-phonon interaction with the breathing distortions as described before.

The existence of polarons or bipolarons trapped at Bi sites in BBO was already theoretically described in Ref. [48]. The difference is that in that work the doping is caused by K substitution at Ba sites. They show that local lattice relaxations are sufficiently large to screen the localized holes and that hole doped BBO remains semiconducting upon moderate hole doping. In this paper, we show that the level of doping with Bi vacancies is 3 to 5 times larger than with K. Notwithstanding this, it is remarkable that the system remains semiconducting for all the concentrations studied.

IV. CONCLUSIONS

We have shown that it is possible to synthesize thin layers of BBO perovskite with a large amount of Bi vacancies. Transport properties were analyzed with a polaronic model and the existence of these defects was theoretically validated. Our DFT calculations performed for Bi-deficient BBO supercells show that Bi vacancies give rise to different type of polarons, depending on the vacancies concentration. After the Bi vacancy is formed, the missing electrons induce polaron and/or bipolarons that consist in one or two holes trapped at some of the remaining Bi sites, or even at the oxygen octahedron surrounding the vacancy for large vacancies concentrations.

We conclude that hole doped BBO remains semiconducting despite the large hole concentration induced by the Bi deficiency. We finally estimate the activated diffusion barrier for all these type of defects to analyze their contribution to the transport properties. We show that the calculated energy barriers of the charges trapped at Bi sites are correlated to the electron-phonon coupling energy scale. The calculated activated barriers for the simulated bulk supercells are somewhat larger than the one obtained from the fit of the transport

experiments. In view of previous theoretical results for other BBO interfaces, these larger values are expected to decrease in confined situations such as the Bi-deficient BBO layer studied in this paper and match the experimentally extracted activation energies. We finally conclude that the polarons trapped at Bi sites strongly contribute to the electrical conductivity of Bi-deficient BBO and, in a more general framework, that the control of Bi vacancies can be used as a tool for tuning the electronic properties of this perovskite.

ACKNOWLEDGMENTS

The authors received financial support from PICTs No. 2015-0869, No. 2016-0867, No. 2017-1836, and No. 2019-02128 of ANPCyT, Argentina. Also, funding from EU-H2020-RISE project “MELON” (SEP-2106565560) is acknowledged. D.R. thanks the Nederlandse Organisatie voor Wetenschappelijk Onderzoek for a visiting grant, Project No. 040.11.735, “Memcapacitive elements for cognitive devices”. We thank D. Vega, from CAC-CNEA, for some of the XRD measurements. We thank B. J. Kooi and B. Noheda for the access to the microscopy facilities at RuG.

-
- [1] J. Coey, M. Viret, and S. von Molnár, *Adv. Phys.* **58**, 571 (2009).
- [2] M. Dawber, K. M. Rabe, and J. F. Scott, *Rev. Mod. Phys.* **77**, 1083 (2005).
- [3] C. N. R. Rao, *Ferroelectrics* **102**, 297 (1990).
- [4] M. Shellaiah and K. W. Sun, *Chemosensors* **8**, 55 (2020).
- [5] A. Sawa, *Mater. Today* **11**, 28 (2008).
- [6] S. Yu, *Neuro-Inspiring Computing Using Resistive Synaptic Devices* (Springer International Publishing, Cham, 2017).
- [7] F. Gunkel, D. V. Christensen, Y. Z. Chen, and N. Pryds, *Appl. Phys. Lett.* **116**, 120505 (2020).
- [8] M.-A. Rose, B. Šmíd, M. Vorokhta, I. Slipukhina, M. Andrä, H. Bluhm, T. Duchoň, M. Ležaić, S. A. Chambers, R. Dittmann *et al.*, *Adv. Mater.* **33**, 2004132 (2021).
- [9] L. F. Mattheiss, E. M. Gyorgy, and D. W. Johnson, *Phys. Rev. B* **37**, 3745 (1988).
- [10] R. J. Cava, B. Batlogg, J. J. Krajewski, R. Farrow, L. W. Rupp Jr, A. E. White, K. Short, J. F. Peck, and T. Kometani, *Nature (London)* **332**, 814 (1988).
- [11] D. Cox and A. Sleight, *Solid State Commun.* **19**, 969 (1976).
- [12] B. J. Kennedy, C. J. Howard, K. S. Knight, Z. Zhang, and Q. Zhou, *Acta Cryst. B* **62**, 537 (2006).
- [13] Z.-X. Shen, P. A. P. Lindberg, B. O. Wells, D. S. Dessau, A. Borg, I. Lindau, W. E. Spicer, W. P. Ellis, G. H. Kwei, K. C. Ott, J. S. Kang, and J. W. Allen, *Phys. Rev. B* **40**, 6912 (1989).
- [14] M. Nagoshi, T. Suzuki, Y. Fukuda, K. Ueki, A. Tokiwa, M. Kiruchi, Y. Syono, and M. Tachiki, *J. Phys.: Condens. Matter* **4**, 5769 (1992).
- [15] K. Foyevtsova, A. Khazraie, I. Elfimov, and G. A. Sawatzky, *Phys. Rev. B* **91**, 121114(R) (2015).
- [16] N. C. Plumb, D. J. Gawryluk, Y. Wang, Z. Ristić, J. Park, B. Q. Lv, Z. Wang, C. E. Matt, N. Xu, T. Shang, K. Conder, J. Mesot, S. Johnston, M. Shi, and M. Radovic, *Phys. Rev. Lett.* **117**, 037002 (2016).
- [17] S. Balandeh, R. J. Green, K. Foyevtsova, S. Chi, O. Foyevtsov, F. Li, and G. A. Sawatzky, *Phys. Rev. B* **96**, 165127 (2017).
- [18] B. Yan, M. Jansen, and C. Felser, *Nat. Phys.* **9**, 709 (2013).
- [19] V. Vildosola, F. Güller, and A. M. Llois, *Phys. Rev. Lett.* **110**, 206805 (2013).
- [20] B. Meir, S. Gorol, T. Kopp, and G. Hammerl, *Phys. Rev. B* **96**, R100507(R) (2017).
- [21] S. Di Napoli, C. Helman, A. M. Llois, and V. Vildosola, *Phys. Rev. B* **103**, 174509 (2021).
- [22] T. Makita and H. Abe, *Jpn. J. Appl. Phys.* **36**, L96 (1997).
- [23] A. Gozar, G. Logvenov, V. Y. Butko, and I. Bozovic, *Phys. Rev. B* **75**, 201402(R) (2007).
- [24] K. Inumaru, H. Miyata, and S. Yamanaka, *Phys. Rev. B* **78**, 132507 (2008).
- [25] H. G. Lee, Y. Kim, S. Hwang, G. Kim, T. D. Kang, M. Kim, M. Kim, and T. W. Noh, *APL Mater.* **4**, 126106 (2016).
- [26] C. Ferreyra, F. Guller, F. Marchini, U. Lüders, C. Albornoz, A. G. Leyva, F. J. Williams, A. M. Llois, V. Vildosola, and D. Rubi, *AIP Adv.* **6**, 065310 (2016).
- [27] C. Ferreyra, F. Marchini, P. Granell, F. Golmar, C. Albornoz, F. Williams, A. Leyva, and D. Rubi, *Thin Solid Films* **612**, 369 (2016).
- [28] M. Zapf, M. Stübinger, L. Jin, M. Kamp, F. Pfaff, A. Lubk, B. Büchner, M. Sing, and R. Claessen, *Appl. Phys. Lett.* **112**, 141601 (2018).
- [29] M. Zapf, S. Elsässer, M. Stübinger, P. Scheiderer, J. Geurts, M. Sing, and R. Claessen, *Phys. Rev. B* **99**, 245308 (2019).
- [30] R. L. Bouwmeester, K. de Hond, N. Gauquelin, J. Verbeeck, G. Koster, and A. Brinkman, *Phys. Status Solidi (RRL)* **13**, 1800679 (2019).
- [31] L. Jin, M. Zapf, M. Stübinger, M. Kamp, M. Sing, R. Claessen, and C.-L. Jia, *Phys. Status Solidi (RRL)* **14**, 2000054 (2020).
- [32] G. Kim, M. Neumann, M. Kim, M. D. Le, T. D. Kang, and T. W. Noh, *Phys. Rev. Lett.* **115**, 226402 (2015).

- [33] S. J. Skinner and J. A. Kilner, *Mater. Today* **6**, 30 (2003).
- [34] M. Kilo, G. Borchardt, B. Lesage, O. Kaïtasov, S. Weber, and S. Scherrer, *J. Eur. Ceram. Soc.* **20**, 2069 (2000).
- [35] See Supplemental Material at <http://link.aps.org/supplemental/10.1103/PhysRevB.104.125307> for additional x-ray diffraction and TEM experiments.
- [36] D. J. Keeble, S. Wicklein, L. Jin, C. L. Jia, W. Egger, and R. Dittmann, *Phys. Rev. B* **87**, 195409 (2013).
- [37] C. M. Brooks, R. B. Wilson, A. Schäfer, J. A. Mundy, M. E. Holtz, D. A. Muller, J. Schubert, D. G. Cahill, and D. G. Schlom, *Appl. Phys. Lett.* **107**, 051902 (2015).
- [38] M. D. Scafetta and S. J. May, *Phys. Chem. Chem. Phys.* **19**, 10371 (2017).
- [39] F. Li, B. A. Davidson, R. Sutarto, H. Shin, C. Liu, I. Elfimov, K. Foyevtsova, F. He, G. A. Sawatzky, and K. Zou, *Phys. Rev. Materials* **3**, 100802(R) (2019).
- [40] A. W. Sleight, *Phys. C* **514**, 152 (2015).
- [41] A. Prakash, P. Xu, A. Faghaninia, S. Shukla, J. W. Ager, C. S. Lo, and B. Jalan, *Nat. Commun.* **8**, 15167 (2016).
- [42] T. Zhao, W. Shi, J. Xi, D. Wang, and Z. Shuai, *Sci. Rep.* **6**, 19968 (2016).
- [43] R. T. Dolloff, *J. Appl. Phys.* **27**, 1418 (1956).
- [44] M. Jaime, H. T. Hardner, M. B. Salamon, M. Rubinstein, P. Dorsey, and D. Emin, *Phys. Rev. Lett.* **78**, 951 (1997).
- [45] $g_d = Nca^3$, where N is the available sites for a jump, c is the defect concentration, and a was defined in the text. See for instance Ref. [61].
- [46] S. Sugai, S. Uchida, K. Kitazawa, S. Tanaka, and A. Katsui, *Phys. Rev. Lett.* **55**, 426 (1985).
- [47] $g_d = 3/8$ taking N equal to 6 and c is estimated considering 1 polaron in the supercell of volume $(4a)^3/4$.
- [48] C. Franchini, G. Kresse, and R. Podloucky, *Phys. Rev. Lett.* **102**, 256402 (2009).
- [49] P. E. Blöchl, *Phys. Rev. B* **50**, 17953 (1994).
- [50] G. Kresse and J. Furthmüller, *Phys. Rev. B* **54**, 11169 (1996).
- [51] G. Kresse and D. Joubert, *Phys. Rev. B* **59**, 1758 (1999).
- [52] We use the following versions of the PAW PBE pseudopotentials: Basv of 06Sep2000, Bid of 06Sep2000 and Os of 07Sep2000, for Ba, Bi and O, respectively.
- [53] J. P. Perdew, S. Burke, and E. Ernzerhof, *Phys. Rev. Lett.* **77**, 3865 (1996).
- [54] J. Heyd, G. E. Scuseria, and M. Ernzerhof, *J. Chem. Phys.* **118**, 8207 (2003).
- [55] A. V. Krugau, O. A. Vydrov, A. F. Izmaylov, and G. E. Scuseria, *J. Chem. Phys.* **125**, 224106 (2006).
- [56] To build this FCC supercell we begin with a $2 \times 2 \times 2$ supercell of the simple cubic perovskite containing 40 atoms in total and we perform several molecular dynamics steps, followed by relaxation, to stabilize the breathing distortion driven by the charge disproportionation. Once this distortion agrees well with the experimental one, we build up again a $2 \times 2 \times 2$ supercell, described within the FCC Bravais lattice.
- [57] The authors will provide the cif files of the relaxed structures on demand. Please contact to the corresponding author.
- [58] C. Franchini, A. Sanna, M. Marsman, and G. Kresse, *Phys. Rev. B* **81**, 085213 (2010).
- [59] G. Henkelman and H. Jónsson, *J. Chem. Phys.* **113**, 9901 (2000).
- [60] Z. P. Yin, A. Kutepov, and G. Kotliar, *Phys. Rev. X* **3**, 021011 (2013).
- [61] R. J. D. Tilley, *Defects in Solids* (John Wiley & Sons, Inc, Hoboken, 2008).